CHAPTER 6 MINOR LOSS CALCULATIONS

Minor losses represent sources of energy depletion along a reach that are not related to friction loss. For example, minor losses are energy losses related to expansions and contractions along a reach, secondary currents, spiral currents, and eddies.

6.1 PURPOSE OF ANALYSIS

As presented in Chapter 5, it was determined that HEC-RAS underestimated total energy loss through a meander bend in the Type I bend by an average 60% and in the Type III bend by approximately 7%. A possible reason for the discrepancy between calculations resulting from physical model measurements and HEC-RAS output is the possibility that HEC-RAS does not account for certain minor losses. HEC-RAS accounts for minor losses due to expansions and contractions along a reach but it does not account for minor losses due to eddies, spiral, and secondary currents. In order to study the significance of minor loss not accounted for in HEC-RAS, a study was completed for the base-line analysis. Minor losses not accounted for during the base-line analysis were secondary and spiral currents. Minor losses due to secondary and spiral currents are known as minor loss due to a meander bend through the rest of the analysis.

6.2 MINOR LOSS DUE TO MEANDER BEND CALCULATIONS

A procedure was developed to calculate minor losses due to a meander bend along the physical model at 8 cfs, 12 cfs, and 16 cfs. The procedure used a series of spreadsheets to determine average velocity, total energy, and friction loss at each cross section. After the average velocity, total energy, and friction loss were calculated at each cross section, total energy loss through each meander bend was calculated along the Type I and Type III bends. Total energy loss through each meander bend was the final variable needed to determine minor loss due to meander bend. The series of spreadsheets is presented later in more detail.

6.3 RESULTS FROM MINOR LOSS DUE TO MEANDER BEND CALCULATIONS

In order to calculate minor loss due to a meander bend, a series of spreadsheets was used to calculate average velocity, total energy, and friction loss at each cross section and total energy loss through each meander bend. This analysis was performed for discharges of 8 cfs, 12 cfs, and 16 cfs.

6.3.1 Average Velocity Results

Average velocity ($\bar{v}$) at each cross section was calculated using Equation 2.2. Results using Equation 2.2 are shown in Table 6.1 for discharges of 8 cfs, 12 cfs, and 16 cfs. Cross-sectional geometry in the Type I and Type III bends was assumed to be trapezoidal.

Table 6.1. $\bar{v}$ Results

XS	$\bar{v}_{8\ cfs}$ (ft/s)	$\bar{v}_{12\ cfs}$ (ft/s)	$\bar{v}_{16\ cfs}$ (ft/s)
0 (U/S)	1.10	1.15	1.32
1	1.13	1.18	1.34
2	1.10	1.17	1.32
3	1.09	1.17	1.34
4	1.10	1.16	1.33
5	1.13	1.19	1.35
6	1.12	1.17	1.33
7	1.09	1.17	1.33
8	1.11	1.14	1.32
9	1.34	1.39	1.58
10	1.73	1.78	2.01
11	1.75	1.77	2.01
12	1.76	1.77	2.03
13	1.76	1.81	2.05
14	1.74	1.75	2.00
15	1.78	1.76	2.03
16	1.70	1.72	1.99
17	1.69	1.69	1.96
18 (D/S)	1.63	1.65	1.92

6.3.2 Total Energy Loss Results

Once average velocity was calculated at each cross section, total energy at each cross section (*H*) was calculated with Equation 2.3. Table 6.2 presents total energy loss for discharges of 8 cfs, 12 cfs, and 16 cfs. Estimates of total energy at each cross section were used to determine the EGL along the Type I and Type III bends.

Table 6.2. *H* Results

XS	$H_{8\ cfs}$ (ft)	$H_{12\ cfs}$ (ft)	$H_{16\ cfs}$ (ft)
0 (U/S)	97.88	98.09	98.21
1	97.85	98.06	98.19
2	97.84	98.05	98.17
3	97.85	98.05	98.17
4	97.83	98.04	98.16
5	97.83	98.04	98.16
6	97.82	98.04	98.16
7	97.83	98.03	98.16
8	97.81	98.04	98.15
9	97.81	98.03	98.15
10	97.82	98.03	98.15
11	97.79	98.01	98.13
12	97.79	98.01	98.12
13	97.79	98.00	98.12
14	97.78	98.00	98.11
15	97.77	97.99	98.11
16	97.76	97.98	98.10
17	97.75	97.97	98.09
18 (D/S)	97.75	97.97	98.08

In order to determine the EGL along each bend, total energy at each cross section was plotted against the cumulative channel distance through the physical model starting at XS18. A linear trend line was interpolated for the plotted series and the slope of the linear trend line was equal to the EGL. Figure 6.1 through Figure 6.3 illustrate graphs used to calculate the EGL at discharges of 8 cfs, 12 cfs, and 16 cfs.

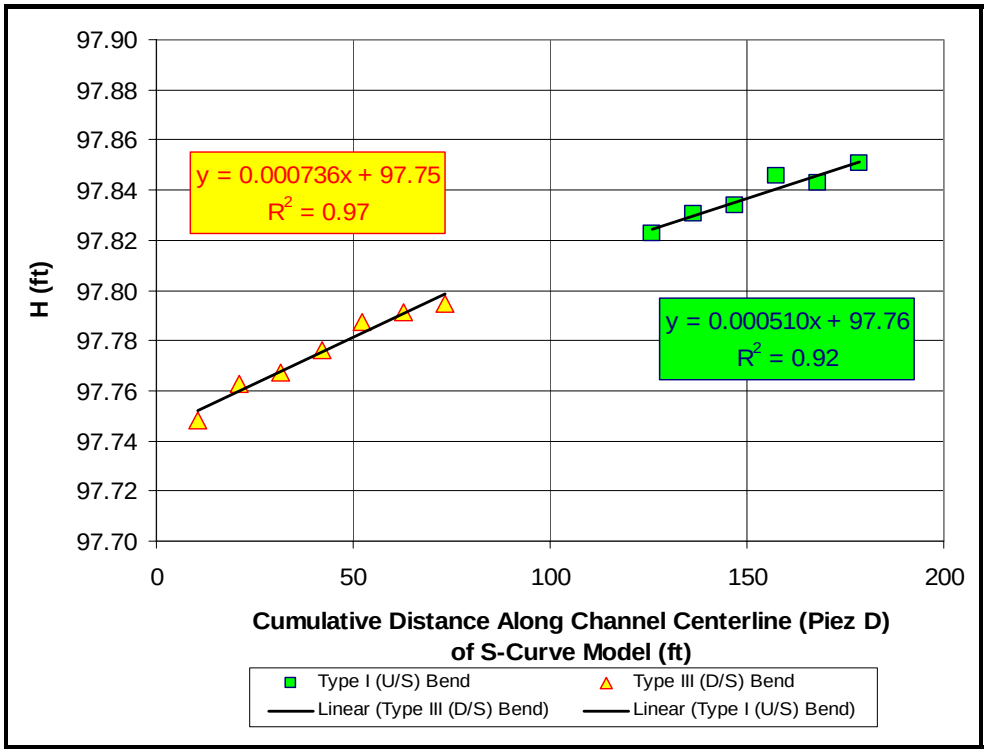

Figure 6.1. Linear Interpolation of Total Energy at 8 cfs

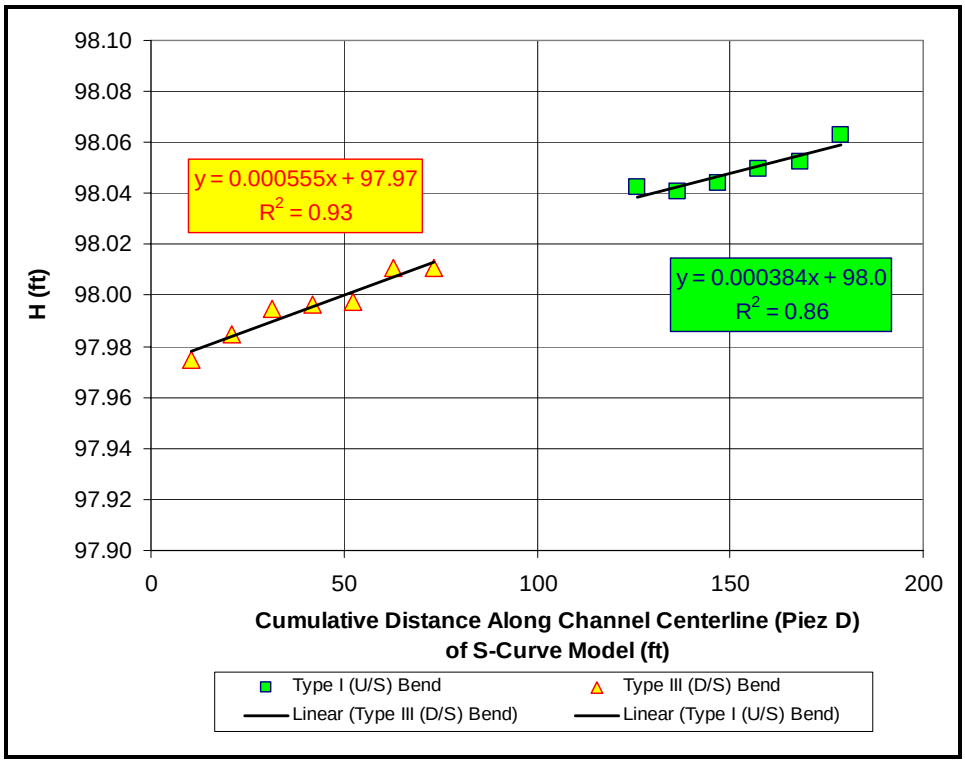

Figure 6.2. Linear Interpolation of Total Energy at 12 cfs

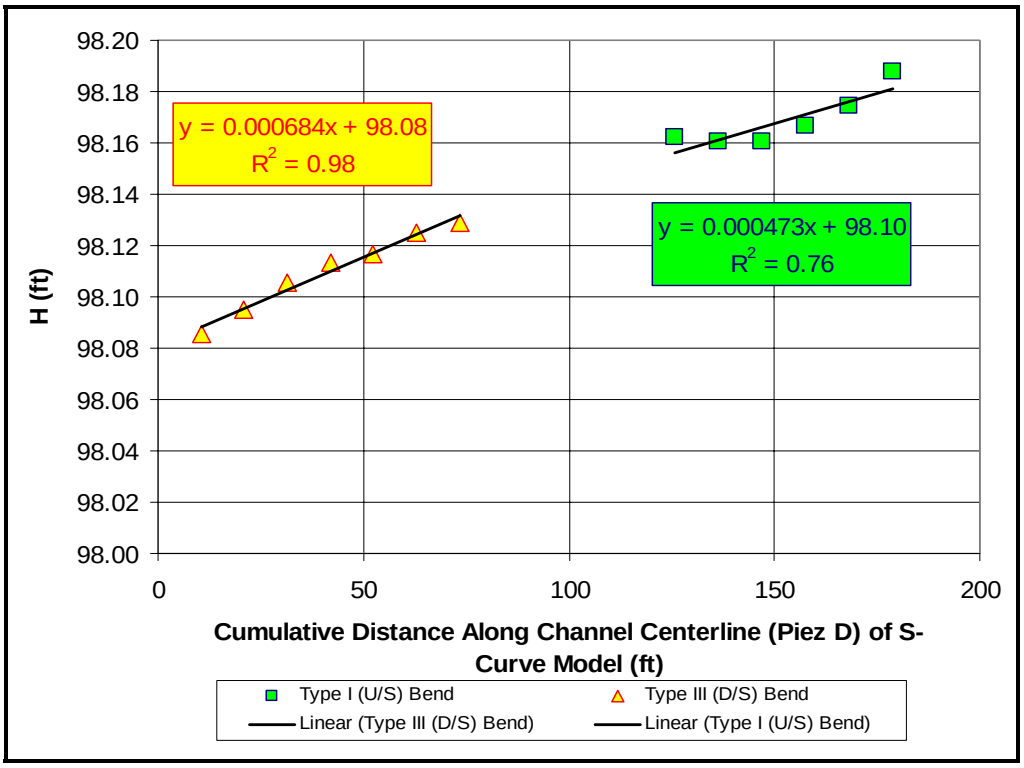

Figure 6.3. Linear Interpolation of Total Energy at 16 cfs

The EGL was used to calculate the average total energy loss between adjacent cross sections ($\bar{h}_t$) in the Type I and Type III bends. Average total energy loss between adjacent cross sections was calculated by multiplying the linear interpolated EGL by the distance between adjacent cross section in the Type I and Type III bends. Table 6.3 presents average total energy loss between adjacent cross sections for discharges of 8 cfs, 12 cfs, and 16 cfs. Average total energy loss between adjacent cross sections was used in the final computation for calculating minor loss due to the meander bends.

Table 6.3. $\bar{h}_t$ Results

Bend	Q (cfs)	Distance Between XS (ft)	EGL (ft/ft)	$\bar{h}_t$ (ft)
Type I (U/S) Bend	8	10.567	0.000510	0.0054
	12		0.000384	0.0041
	16		0.000473	0.0050
Type III (U/S) Bend	8	10.484	0.000736	0.0077
	12		0.000555	0.0058
	16		0.000684	0.0072

6.3.3 Friction Loss Results

Average friction loss between adjacent cross sections (h_{Sf}) was calculated by the average conveyance method. Average conveyance method, defined in Equation 2.10, was the equation used to calculate average friction loss between adjacent cross sections in this analysis since it is the default method in HEC-RAS. Results of average friction loss between adjacent cross sections are shown in Table 6.4 for discharges of 8 cfs, 12 cfs, and 16 cfs. Intuitively, average friction loss between adjacent cross sections in the Type I or Type III bends should be fairly uniform along a prismatic, concrete, rigid boundary, meander bend. This assumption is reflected by the average friction loss between adjacent cross sections calculated in the Type I and Type III bends. For instance, average friction losses between adjacent cross sections results presented in Table 6.4 show similar results for XS0 through XS7.

Table 6.4. h_{Sf} Results

XS	h_{Sf8cfs} (ft)	$h_{Sf12cfs}$ (ft)	$h_{Sf16cfs}$ (ft)
0 (U/S)	0.0024	0.0019	0.0021
1	0.0024	0.0019	0.0021
2	0.0023	0.0019	0.0021
3	0.0023	0.0019	0.0021
4	0.0024	0.0019	0.0022
5	0.0025	0.0019	0.0022
6	0.0024	0.0019	0.0021
7	0.0024	0.0018	0.0021
8	0.0029	0.0022	0.0025
9	0.0047	0.0036	0.0040
10	0.0066	0.0049	0.0055
11	0.0068	0.0049	0.0056
12	0.0069	0.0050	0.0057
13	0.0068	0.0049	0.0056
14	0.0069	0.0048	0.0055
15	0.0066	0.0046	0.0055
16	0.0061	0.0044	0.0052
17	0.0058	0.0042	0.0050
18 (D/S)			

Since the average friction loss is fairly uniform in the Type I and Type III meander bends, a cross-sectional average, average friction loss ($\overline{h}_{Sf}$) was calculated for the Type I and Type III meander bends. Table 6.5 presents cross-sectional average, average friction loss for the Type I and Type III bends for discharges of 8 cfs, 12 cfs, and 16 cfs. Cross-sectional average, average friction loss was used in the final spreadsheet computation for calculating minor loss due to the meander bends.

Table 6.5. $\bar{h}_{Sf}$ Results

Bend	Q (cfs)	$\bar{h}_{Sf}$ (ft)
Type I (U/S) Bend	8	0.0024
	12	0.0019
	16	0.0021
Type III (U/S) Bend	8	0.0066
	12	0.0047
	16	0.0054

6.3.4 Minor Loss Due To Meander Bend Results

Once average total energy loss between adjacent cross sections and cross-sectional average, average friction loss were determined, a spreadsheet analysis was needed to calculate the cross-sectional average minor loss due to meander bends ($\bar{h}_{BEND}$). Cross-sectional average minor loss due to meander bends is calculated by the following equation:

$$\bar{h}_{BEND} = \bar{h}_t - \bar{h}_{Sf} \qquad \textbf{Equation 6.1}$$

where:

$\bar{h}_{BEND}$ = cross-sectional average minor loss due to meander bend (ft);

$\bar{h}_{Sf}$ = cross-sectional average, average friction loss (ft); and

$\bar{h}_t$ = cross-sectional average total energy loss (ft).

Equation 6.1 assumes that minor loss due to expansions and contractions is negligible compared to the energy loss due to friction and meander bends. Table 6.6 presents the calculations of cross-sectional average minor loss due to meander bends for the Type I and Type III bends at discharges of 8 cfs, 12 cfs, and 16 cfs.

Table 6.6. $\bar{h}_{BEND}$ Results

Bend	Q (cfs)	Distance Between XS (ft)	Energy Grade Line (ft/ft)	$\bar{h}_t$ (ft)	$\bar{h}_{Sf}$ (ft)	$\bar{h}_{BEND}$ (ft)
Type I (U/S) Bend	8	10.567	0.000510	0.0054	0.0024	**0.0030**
	12		0.000384	0.0041	0.0019	**0.0021**
	16		0.000473	0.0050	0.0021	**0.0029**
Type III (U/S) Bend	8	10.484	0.000736	0.0077	0.0066	**0.0012**
	12		0.000555	0.0058	0.0047	**0.0011**
	16		0.000684	0.0072	0.0054	**0.0017**

Once cross-sectional average minor loss due to meander bends was calculated, it was important to determine the average minor loss due to meander bends through the meander bend ($\bar{h}_{BEND-TOTAL}$); in this case, through the Type I and Type III bends. Average minor loss due to meander bends through a meander bend was calculated by the following equation:

$$\bar{h}_{BEND-TOTAL} = \bar{h}_{BEND} * \left(XS_{TOTAL} - 1\right) \qquad \textbf{Equation 6.2}$$

$\bar{h}_{BEND}$ = average minor loss due to a meander bend between adjacent cross sections (ft);

$\bar{h}_{BEND-TOTAL}$ = average minor loss due to the meander bend through the bend (ft); and

XS_{TOTAL} = number of significant cross sections used in analysis.

Six cross sections were used in the Type I bend and seven cross sections were used in the Type III bend to calculate Equation 6.2. In the Type I bend, eight cross sections are marked along the physical model but XS0, XS7, and XS8 were excluded from the calculation in order to eliminate the influence from the head box and transition section. In the Type III bend, eight cross sections are marked along the physical model but XS10 and XS18 were excluded from the calculation in order to eliminate the influence from the

transition section and the stop logs. Results of average minor loss due to meander bends through a meander bend is shown in Table 6.7 for discharges of 8 cfs, 12 cfs, and 16 cfs.

Table 6.7. $\bar{h}_{BEND\text{-}TOTAL}$ Results

Bend	Q (cfs)	$\bar{h}_{BEND}$ (ft)	Number of Cross Sections	$\bar{h}_{BEND-TOTAL}$ (ft)
Type I (U/S) Bend	8	0.0030	6	0.0149
	12	0.0021	6	0.0107
	16	0.0029	6	0.0143
Type III (U/S) Bend	8	0.0012	7	0.0069
	12	0.0011	7	0.0068
	16	0.0017	7	0.0104

This technique was also used to determine the average friction loss through the meander bend ($\bar{h}_{Sf-TOTAL}$) and the average total energy loss through the meander bend ($\bar{h}_T$). Once these values were calculated, it was important to determine how significant average minor loss due to a meander bend through each meander bend was to the average total energy loss through the bend computation. Percent energy loss due to average minor loss due to a meander bend through each meander bend is presented in Table 6.8. Table 6.8 shows that at 16 cfs, average minor loss due to a meander bend through each meander bend is 57% of average total energy loss through the meander bend in the Type I bend. In the Type III bend the percentage is not as high but it still estimates that 24% percent of average total energy loss through the meander bend in the Type III bend is due to average minor loss due to a meander bend through each bend. Since 57% of average total energy loss through the meander bend is due to average minor loss due to a meander bend through the bend in the Type I bend and 24% of average total energy loss through the meander bend is due to average minor loss due to a meander bend through the

meander bend in the Type III bend, it is evident that spiral and secondary currents are significant in total energy loss calculations. The difference between the percentage of energy loss due to the meander bend in the Type I bend versus the Type III bend demonstrates that the radius of curvature in each bend plays a significant role in determining average minor loss due to a meander bend through each meander bend.

Table 6.8. Percent Energy Loss Due to $\bar{h}_{BEND\text{-}TOTAL}$

Bend	Q (cfs)	$\bar{h}_T$ (ft)	$\bar{h}_{Sf-TOTAL}$ (ft)	$\bar{h}_{BEND-TOTAL}$ (ft)	% Energy Loss Due to $\bar{h}_{BEND-TOTAL}$
Type I (U/S) Bend	8	0.0269	0.0121	0.0149	**55**
	12	0.0203	0.0096	0.0107	**53**
	16	0.0250	0.0107	0.0143	**57**
Type III (U/S) Bend	8	0.0463	0.0394	0.0069	**15**
	12	0.0349	0.0281	0.0068	**20**
	16	0.0430	0.0326	0.0104	**24**

6.4 CONCLUSION

Since this analysis demonstrated that average minor loss due to meander bends through a meander bend was significant in the physical model, a technique needed to be developed in order to calculate average minor loss due to meander bends through a meander bend with HEC-RAS output. One such technique was developed in order to examine flow in a bend prior to adding structures. This technique is further discussed in Chapter 7.